Progress in Medical Devices
eISSN: 2957-5443

Zentime

Research Article https://doi.org/10.61189/299269sghbqx

Design and simulation of a multi-functional radiofrequency tissue welding electrode

Wanwen Yang, Lin Mao, Yilong Chen, Chengli Song

Shanghai Institute for Minimally Invasive Therapy, School of Health Science and Engineering, University of Shanghai for Science and Technology, China, 200093

Corresponding author: Lin Mao.

Declaration of conflict of interest: None.

Received August 21, 2023; Accepted December 6, 2023; Published December 31, 2023

Highlights

- Two novel electrodes (one with circle surface and the other with square and arched surface) were designed for radiofrequency intestinal anastomosis, and their effects were compared to a control electrode (smoot surface).
- The temperature and thermal damage to tissue produced by the two designed electrodes during welding are lower than those by the control electrode.
- The electrode with square and arched surface has a smaller effective welding area and better effect on intestinal anastomosis.

Abstract

Purpose: To explore the effect of electrode structure on welding quality by modifying the structure of magnesium alloy electrode. **Methods:** Two novel electrodes were designed in this study, including one with a circle (C) surface and the other with a square and arched (SA) surface. The designed electrodes were compared to a control electrode with a smooth surface in terms of temperature distribution, thermal damage to tissue, and effective welding area. Finite element analysis was used to analyze the stress and strain of all electrodes and thermal damage to the tissue. **Results:** Pressure applied to the designed electrodes was within the elastic limit, and the deformation was less than 1%. The highest temperature of SA electrode (99.6 ℃) was similar to that of the control (100 ℃), while that of C electrode (106 ℃) was higher than the control. The mean temperature at the welding site in intestine of the control electrode was significantly higher than that of the other two electrodes. Besides, the mean temperature of C electrode was also slightly higher than that of SA electrode. The tissues welded by the control electrode, C electrode and SA electrode were completely necrotic within an axial distance of 2.546 mm, 2.079 mm, and 1.835 mm from the edge of the welding area, respectively. **Conclusion:** SA electrode has the lowest thermal damage compared with the other two electrodes due to smaller effective welding area. Therefore, SA electrode is better than the other two electrodes.

Keywords: Radiofrequency energy, electrode structure, anastomosis, thermal damage

I. Introduction

In 2020, the Global Cancer Statistics Report stated that colorectal cancer is a highly prevalent cancer, and its incidence and mortality are among the top five of all cancers [1]. Clinically, the primary treatment methods for colorectal cancer include surgery, radiation therapy, chemotherapy, and targeted therapy [2]. Surgical resection is a predominant treatment approach that widely used in all stages of colorectal cancer [3].

Surgical site infections (SSIs) are one of the most common complications after surgery, with implications for both clinical outcomes and medical costs [4, 5]. The incidence of SSIs due to large quantity and complexity of bacteria in the colorectal intestinal lumen ranges from 3% to 26%, representing a significant factor contributing to deterioration and death of patients [6-8]. Anastomotic leakage, bleeding, and disruption of incision are the independent risk factors for SSIs in colorectal cancer [9]. Therefore, a safe and reliable anastomosis method plays a significant role in surgical treatment efficacy.

Address correspondence to: Lin Mao, Shanghai Institute for Minimally Invasive Therapy, School of Health Science and Engineering, University of Shanghai for Science and Technology, NO.516 Jungong Road, Yangpu District, Shanghai 200093, China. Tel: +86-21-55572159. E-mail: linmao@usst.edu.cn.

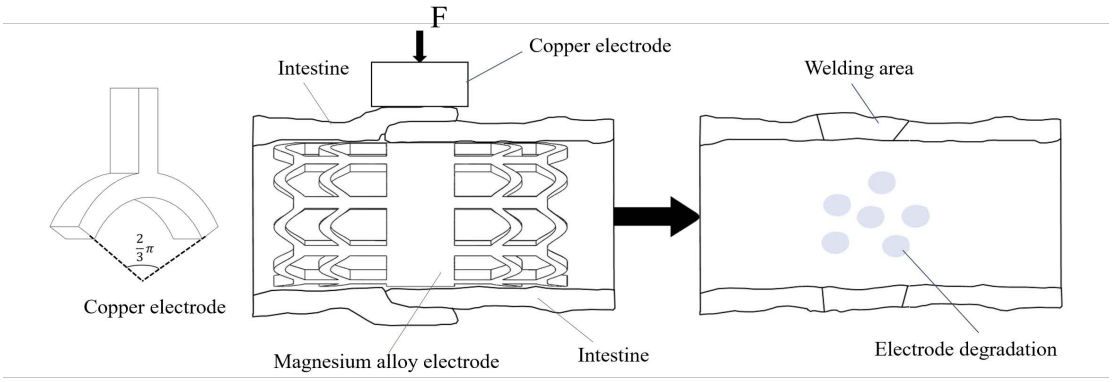

Figure 1. Working process of novel electrode.

Suturing and stapling are two conventional intestinal anastomosis techniques [10]. Both of them are discontinuous tissue matching. Consequently, complications such as anastomotic leakage and bleeding often occur [11]. With the further development of medical technology, anastomosis techniques have gradually evolved towards minimally invasive surgery. Biological adhesives, energy welding, and other technologies have been gradually applied in anastomosis [12]. However, common biological adhesives have problems such as poor adhesive elasticity, strong tissue toxicity, and rejection reaction. As a result, bio-adhesives are difficult to be used widely [13, 14]. The energy-based tissue fusion technology suggests that tissue healing can be achieved by heating the tissue with energy such as light, electricity, acoustic waves to coagulate and bind the proteins in the tissues at welding site [15-17].

With the progress of electrosurgical technology, researchers have found that while heating the tissue, the triple helical structure of type I collagen monomers uncoils and transmutes to a randomly coiled mass of peptide chains [18]. The peptide chains solidify into a fused mass while two tissue layers are compressed together [19]. In 2006, Salameh et al. used LigaSure system to suture blood vessels, which was the first application of radiofrequency (RF) energy for anastomosis [20]. In 2014, Zhou et al. explored the feasibility and effectiveness of intestinal anastomosis in an in vitro porcine model with high-frequency welding device [21]. However, this technology has been hindered due to problems such as tissue thermal damage and insufficient anastomotic strength. Henceforth, a series of studies have been conducted to continuously improve the welding quality of intestinal tissue by altering the processing parameters such as extrusion pressure, welding temperature, duration of heat, and electrode structure [22, 23]. In 2015, Zhao et al. studied the effect of electrode structure and pressure on anastomosis in isolated pigs and showed that an optimized electrode structure could contribute to the anastomosis outcome [24]. In 2019, Tu et al. changed control parameters (power, interval time, and terminal impedance) to investigate the effect on the anastomotic quality [25].

Based on previous studies, we designed two types of electrodes and analyzed the influence of the electrode structure on the anastomotic quality. To explore the effect of electrode structure on welding quality, mechanical simulation was initially used to verify the mechanical properties of all electrodes. Then, various temperatures and thermal damages were calculated through electrothermal simulation.

II. Materials and methods

Mechanical structure design

In this study, magnesium alloy was selected as the material of welding electrodes (negative electrode). Magnesium alloy has high biocompatibility and is biodegradable in vivo. Excessive magnesium produced by degradation can be eliminated through the excretion system without metal aggregation, which is conducive to the formation of an intestinal anastomosis free of foreign bodies.

The working process of the novel electrodes is displayed in **Figure 1**. Magnesium alloy electrode is placed in the intestine as a negative electrode which can degrade in the intestine. Two separate segments of intestinal tissue were overlapped in the order of “mucosa-serosa”. Then, a copper electrode consisting of three identical discrete copper electrodes, each spanning at an angle of 120 degrees (**Figure 1**, left), was placed above the anastomotic area as positive electrode. RF energy was applied to

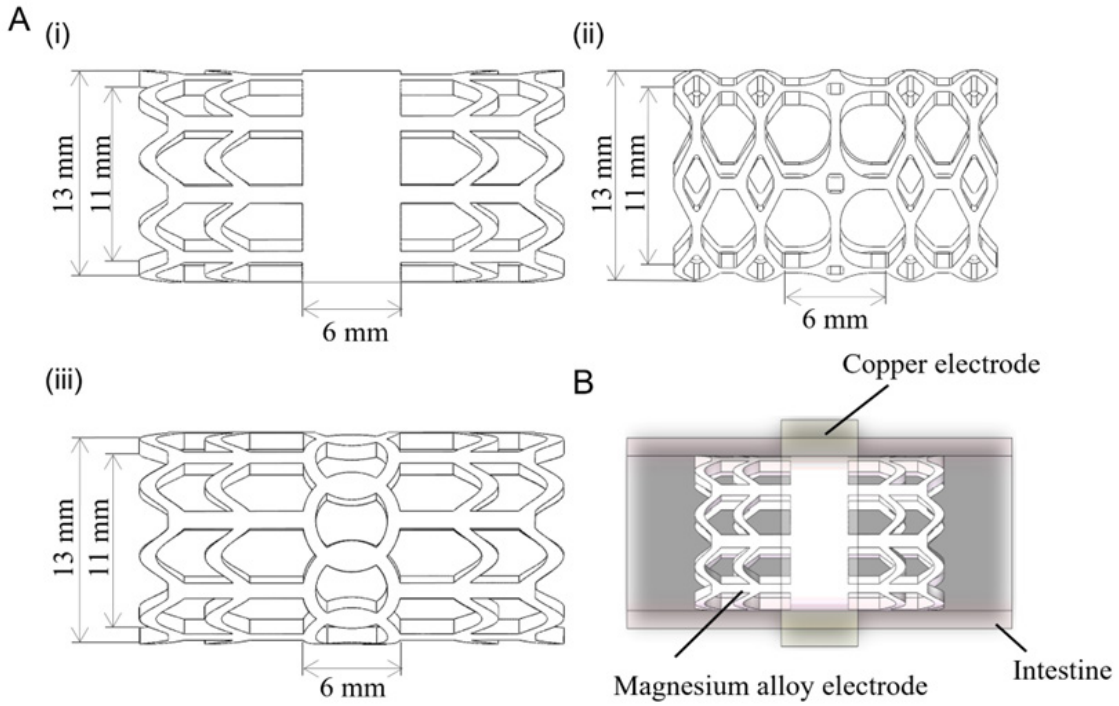

Figure 2. Designed electrode structures and simulation model of control group. (A) Structures of control electrode (i), SA electrode (ii) and C electrode (iii); (B) Simulation model of control group. SA, square and arched; C, circle.

complete the welding. The positive electrode was removed after welding, and the negative electrode could degrade in the intestine.

The welding quality can be affected by the electrode structure of the welding area. Therefore, the differences of electrodes mainly lie in the welding area. During structural design, effective welding area, the contact area between the electrode and intestine in the welding area, and continuous symmetrical structure were considered. SOLIDWORKS 2022 software was used for the design of the mechanical structure. The three designed electrodes are shown in **Figure 2A**. An electrode with a smooth surface in the welding area was used as a control electrode, with an effective welding area of 245.04 mm^2. Additionally, we designed two electrodes: one is the circle (C) electrode whose welding part is composed of successive rings; the other is the square and arched (SA) electrode whose welding part is formed of the continuous pattern with square inside and surrounded by four C arcs. The effective welding areas of these two electrodes are 136.21 mm^2 and 96.27 mm^2, respectively. Besides, for all electrodes, the inner diameter is 11 mm, and the outer diameter is 13 mm. Width of the welding area is 6 mm. The structure of both electrodes can be referred to the control electrode.

Taking the control electrode as an example, the assembly drawing is shown in **Figure 2B**, and the same structure was used for the copper electrodes in the tissue fusion with the three electrodes.

Finite element analysis

Mechanical simulation

Construction of model

Mechanical properties alter due to the difference of electrode structure. Therefore, static structural module of ANSYS Workbench software was used to analyze the stress and strain of the three electrodes under pressure. Tetrahedron mesh was applied in this simulation. Element size was set to 0.5 mm. The material parameters in the simulation are shown in **Table 1**.

Boundary conditions

Both ends of the intestine were fixed. According to our previous studies, a force of 20 N was applied through the positive electrode, which was converted to a pressure of 0.125 MPa in the simulation [26]. The contact interaction between the electrode and the intestine was seen as friction, with a friction coefficient of 0.1.

Electrothermal simulation

Table 1. Mechanical parameters

Project	Density (kg/m^3)	Young's modulus (Pa)	Poisson's ratio
Copper	8960	1.25e11	0.345
Magnesium alloy	1770	4.2e10	0.35
Intestine	1030	1.6e6	0.493

Table 2. Electrothermal parameter

Project	Density (kg/m^3)	Electrical conductivity (S/m)	Thermal conductivity (W/(m·K))	Thermal capacity (J/(kg·K))	Relative dielectric constant (1)
Magnesium alloy	1770	6.417e6	105.224	1e3	1
Copper	8960	5.998e7	400	385	1
Intestine	1030	0.07	0.493	3.595e3	8.98e3

Construction of model

The trend of temperature variation and distribution as well as the thermal damage were analyzed by alternating current/direct current (AC/DC) module and heat transfer module of COMSOL5.6. One-third of each electrode model was applied to the electrothermal simulation because of the symmetry of electrode structure. Specific thermodynamic parameters of the material in simulation are shown in **Table 2** [27-29]. Free Tetrahedral meshes were applied in the simulation. The quantity of meshes of the control electrode, C electrode and SA electrode were 38143, 46264, and 390151, respectively.

Governing equations

The viscoelastic properties of intestinal tissue were calculated by the Maxwell model expressed in equation 1,

$$\dot{\varepsilon} = \frac{\dot{\sigma}}{E} + \frac{\sigma}{\eta} \quad (1)$$

where ε is strain, σ is stress, E is elastic modulus, and η is viscosity coefficient [30].

The thermoelectric coupling problem followed the Pennes biological heat transfer equation 2,

$$\rho c \frac{\partial T}{\partial t} + \nabla \cdot (k \nabla T) + \rho_b c_b \omega (T_b - T) + Q \quad (2)$$

where ρ represents density, c represents specific heat, k represents thermal conductivity, T represents temperature, represents arterial temperature, represents blood density, represents blood specific heat, represents blood perfusion rate, and Q represents power absorption [31].

Tissue thermal damage was calculated using the Arrhenius equation expressed in equation 3,

$$\Omega(\tau) = \int_0^\tau A e^{-\frac{E_a}{RT}} dt \quad (3)$$

where denotes the degree of tissue injury, denotes heating time, A denotes frequency factor, and denotes activation energy [32].

Boundary conditions

RF power was converted to the corresponding root mean square value of the DC voltage to enhance the convergence of the finite element model. The energy input to the positive electrode was 110 V AC, while that to the magnesium alloy electrode was set to 0. Domain point probes were added to detect temperature changes, and boundary probes were added to observe thermal damage in the intestine. The time of simulation was 8 s. At t=0, the initial tissue temperature was set to 37 °C, and the environment temperature was set to 25 °C.

III. Results

Mechanical simulation

Nephograms of the designed electrodes are presented in **Figure 3**. The maximum stresses of the control electrode, C electrode and SA electrode were 1.22 MPa, 6.69 MPa and 3.09 MPa, respectively. The maximum stresses of all three electrodes were much less than the yield strength (175 MPa) of magnesium alloy. The maximum strain of C electrode was 0.00016, which is negligible.

Electrothermal simulation

Only part of each electrode was applied to the electrothermal simulation because of the symmetry structure of electrode. The surface diagrams of the temperature at the 8th second for each electrode model are presented in **Figure 4**. The highest temperature of control electrode, C electrode, and SA electrode were 100 ℃, 106 ℃ and 99.6 ℃, respectively.

In order to analyze the temperature variation of the welding area more specifically, the mean

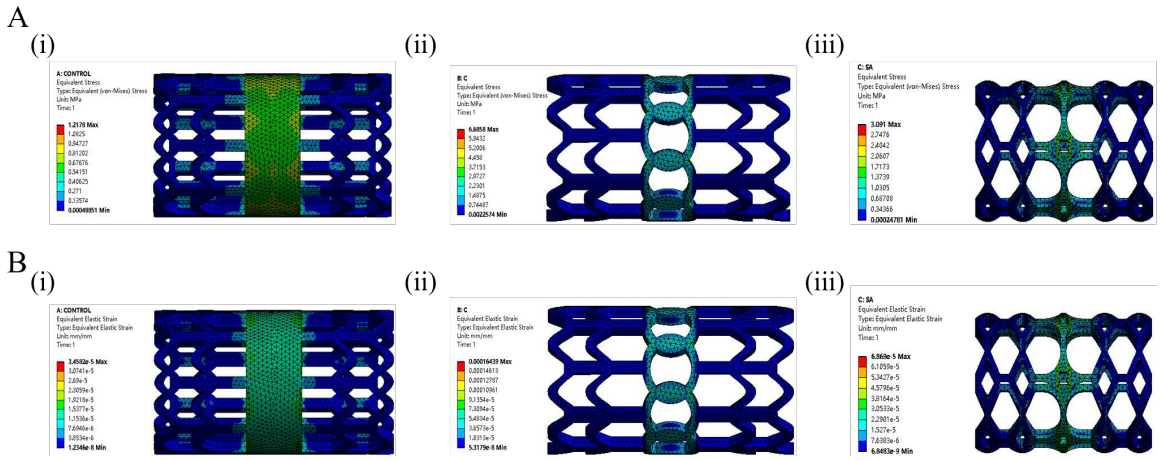

Figure 3. Nephograms of mechanical simulation of the three electrodes. (A) Stress nephogram of control electrode (i), C electrode (ii) and SA electrode (iii). (B) Strain nephogram of control electrode (i), C electrode (ii) and SA electrode (iii). C, circle; SA, square and arched.

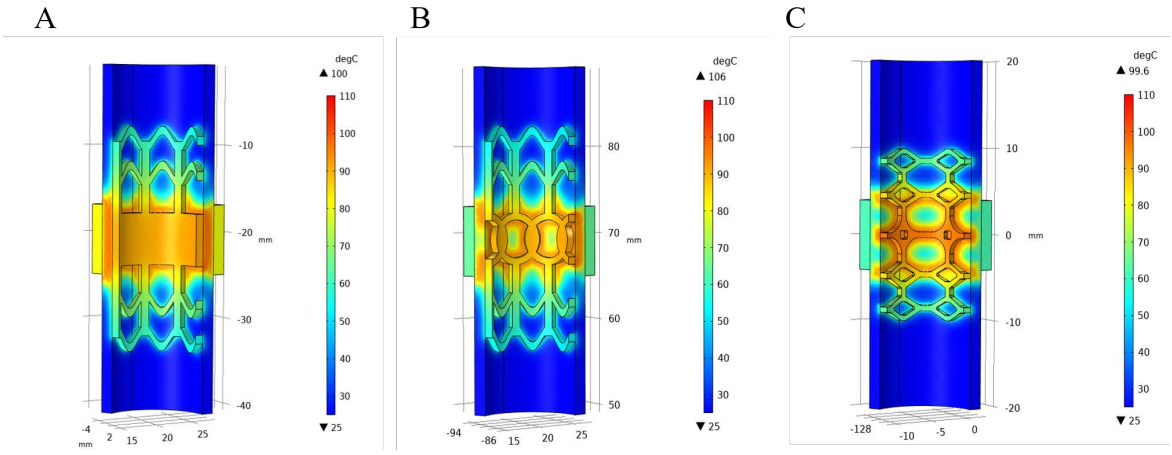

Figure 4. Temperature distributions in the three electrode models. (A) Control electrode; (B) C electrode; (C) SA electrode. C, circle; SA, square and arched.

temperature variation in the intestine for all electrode models is shown in **Figure 5B**. From the 4th second, the mean temperature growth rate at the welding site of intestine in all three electrode models increased significantly. The mean temperature of the control electrode model was the highest and that of C electrode model was the lowest.

Two points in the intestine were specifically selected to insert temperature probes to detect the temperature variation of intestine during the process of welding, which are shown in **Figure 5A**. The mean temperature variations of point a and point b in the intestine are shown in **Figure 5C**. The temperature at point a of the control electrode was the highest and that of C electrode was the lowest. Point b of the three electrode models had the same result. The temperature of point a and b was the same for control electrode, while the temperature of point b was higher than that of point a for C electrode and SA electrode.

In addition, tissue necrosis is one of the important factors to measure the anastomosis effect. As shown in **Figure 6A**, the tissues welded by the control electrode, C electrode, and SA electrode were completely necrotic within an axial distance of 2.546 mm, 2.079 mm, and 1.835 mm from the edge of the welding area, respectively. More tissue survived in the welding area of SA electrode than the other two electrodes. **Figure 6B** shows the proportion of necrotic tissue in all three electrode models. The proportion of necrotic tissue was the highest in the control electrode model and lowest in the SA electrode model. Furthermore, the proportion of necrotic tissue of all electrode models increased sharply from the 4th second.

IV. Discussion

Intestinal reconstruction is an important step in intestinal surgery, which is one of the cornerstones of visceral surgery and is not expected to be overcome or replaced by other treatments soon [33]. Traditional anastomosis includes

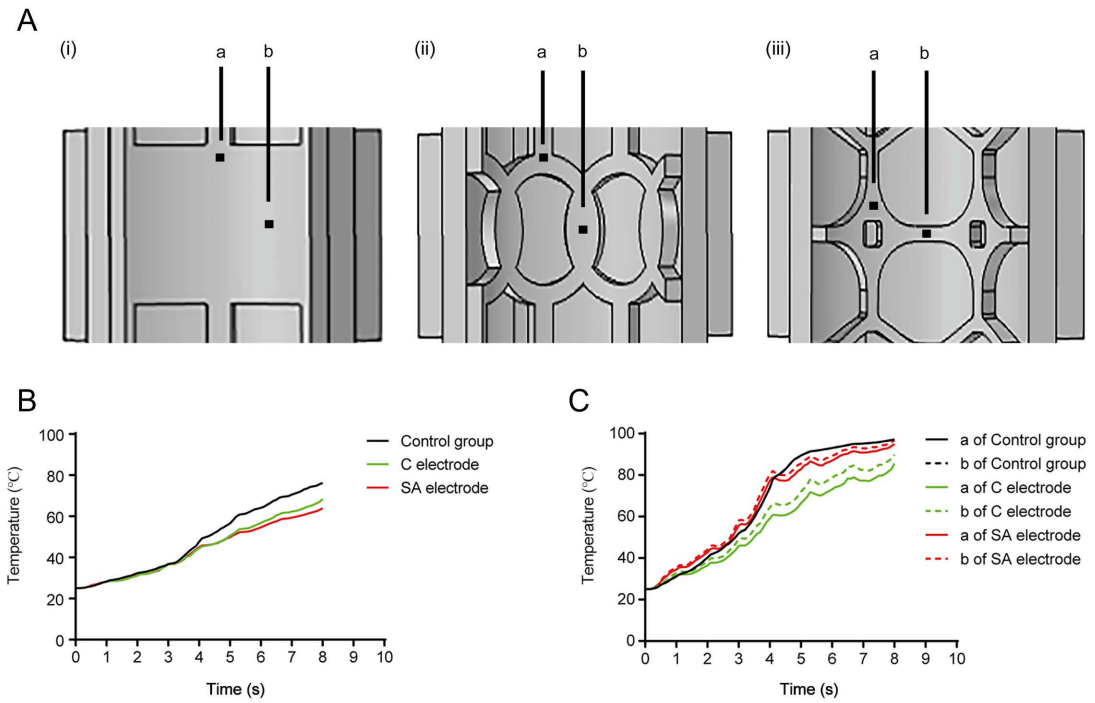

Figure 5. Mean temperature variation at welding site of intestine in all electrode models. (A) Domain point positions at intestine of the control electrode (i), C electrode (ii) and SA electrode (iii); (B) Mean temperature variation at the welding site of intestine in all three electrode models; (C) Temperature variation of probes at intestine in all three electrode models. C, circle; SA, square and arched.

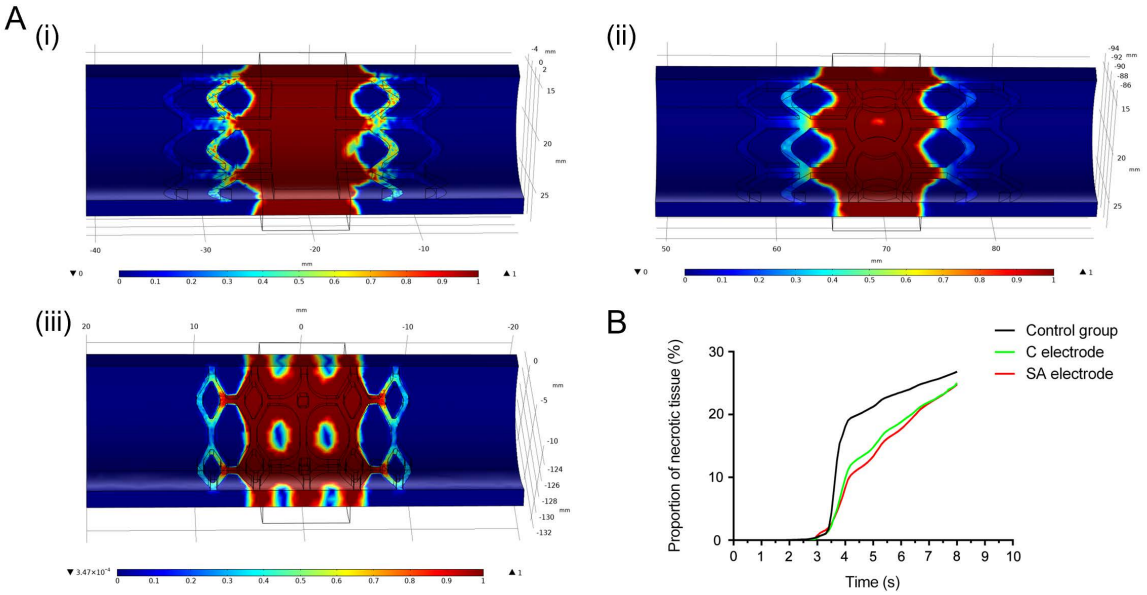

Figure 6. Tissue necrosis in the three electrode models. (A) Nephogram of proportion of necrotic tissue of Control group (i), C electrode (ii) and SA electrode (iii) at the 8th second; (B) Proportion of necrotic tissue. C, circle; SA, square and arched.

suturing and stapling. The former is not suitable for minimally invasive surgery, and the latter may cause inflammation and infection, which is not conducive to anastomosis healing. Therefore, energy tissue fusion technology has emerged for intestine anastomosis.

However, intestinal leakage has always been a challenge after thermal anastomosis. Pressure, welding time, and temperature during welding are important factors that affect the anastomosis effect. In previous studies, pressure, welding time, and other experimental parameters were explored to enhance the burst pressure and reduce thermal damage [21, 25]. Ritcher et al. studied the effects of 4 different electrodes on vascular closure with RF energy, which indicated the importance role of electrode structure in tissue welding [34]. However, there are still few reports to date on RF tissue welding technology

from the perspective of electrode structure [24]. Therefore, in this study, we aimed to investigate the effect of different electrode structure on welding quality to fill in the research gap in this respect. Previous studies of our team did lots of experiments in vivo and obtained optimized parameters of pressure and welding time, which were applied into simulations in the models [26]. C electrode and SA electrode were designed to reduce the thermal damage in the welding area, enhance the thermal diffusion ability, and improve the healing ability of the intestinal tissue. In fact, changing the electrode structure of welding area to decrease effective welding area can reduce necrotic tissues and improve heat dissipation capacity.

The maximum stress (6.69 MPa) of the C electrode was the largest in all electrodes, which was much less than the yield strength (175 MPa) of magnesium alloy. Besides, the maximum strain of the C electrode, 0.00016, was much less than 1%. Therefore, the mechanical properties of the SA electrode are better than that of the C electrode, but the mechanical properties of all electrodes are acceptable. Of course, excessive pressure will affect the intestinal tissue and reduce the quality of the anastomotic stoma.

The highest temperature of the C electrode was 6 ℃, higher than that of the control electrode. This is due to the hollow structure, which reduces effective welding area, thus increases the local current density. The highest temperature of the SA electrode (99.6 ℃) was similar to that of the control electrode (100 ℃). The effective welding area (96.27 mm^2) of the SA electrode was about 39.29% of the effective welding area of the control. The effective welding area (136.21 mm^2) of the C electrode was about 55.59% of that of the control. That is to say, the hollow area is large enough, so the heat dissipation rate of the SA electrode is faster than the C electrode. These results correspond to the mean temperature variation at the intestine of the welding area in three electrode models. The mean temperature of the SA electrode was the lowest and that of control electrode was the highest due to the hollow structure.

The mean temperature was calculated to analyze the whole temperature variation of intestine in the welding area. Therefore, temperature probes were inserted into two different points of intestine in the welding area. When the input energy was constant, a larger proportion of effective area led to higher temperatures in the entry part. Point a is close to the hollow part and point b is at the connection of electrode symmetric structures in the welding area. In consequence, the temperature of point b of the two novel electrodes were higher than that of point a. Besides, as getting closer to the electrode entity, there is more necrotic tissue in the welding area. Therefore, the rate of tissue necrosis in the SA electrode model was the lowest compared with the other two electrode models.

V. Conclusion

Two novel electrodes (C and SA electrodes) were designed in this study to investigate the effects of electrode structure on RF tissue welding. Finite element analysis was used to analyze the mechanical property of designed electrodes and thermal damage to tissue, which are important indices to evaluate the welding quality. The results of simulations show that the SA electrode is better than the C electrode, and also provide a strong support for facilitating RF tissue welding technology by optimizing electrode structures. Even so, further in vitro and in vivo experiments are required to ensure the feasibility and safety of this technology.

References

[1] Hyuna S, Jacques F, L. SR, et al. Global Cancer Statistics 2020: GLOBOCAN Estimates of Incidence and Mortality Worldwide for 36 Cancers in 185 Countries. CA Cancer J Clin 2021;71:209-249.

[2] Esmeeta A, Adhikary S, Dharshnaa V, et al. Plant-derived bioactive compounds in colon cancer treatment: An updated review. Biomed Pharmacother 2022;153:113384.

[3] Grass F, Behm KT, Duchalais E, et al. Impact of delay to surgery on survival in stage I-III colon cancer. Eur J Surg Oncol 2020;46:455-461.

[4] Broex ECJ, Asselt ADIv, Bruggeman CA, et al. Surgical site infections: how high are the costs? J Clin Med 2022;11:6991.

[5] Kolasiński W. Surgical site infections–review of current knowledge, methods of prevention. Pol J Surg 2019;91:41-47.

[6] Schoetz Jr DJ, Roberts PL, Murray JJ, et al. Addition of parenteral cefoxitin to regimen of oral antibiotics for elective colorectal operations. A randomized prospective study. Ann Surg 1990;212:209-212.

[7] Biondo S, Kreisler E, Fraccalvieri D, et al. Risk factors for surgical site infection after elective resection for rectal cancer. A multivariate analysis on 2131 patients. Colorectal Dis 2012;14:e95-e102.

[8] Smith RL, Bohl JK, McElearney ST, et al. Wound infection after elective colorectal resection. Ann Surg 2004;239:599-607.

[9] Xu Z, Qu H, Kanani G, et al. Update on risk factors of surgical site infection in colorectal cancer: a systematic review and meta-analysis. Int J Colorectal Dis 2020;35:2147-2156.
[10] Holmer C, Winter H, Kroger M, et al. Bipolar radiofrequency-induced thermofusion of intestinal anastomoses--feasibility of a new anastomosis technique in porcine and rat colon. Langenbecks Arch Surg 2011;396:529-533.
[11] Hyman NH. Managing anastomotic leaks from intestinal anastomoses. Surgeon 2009;7:31-35.
[12] Wu Z, Vakalopoulos K, Kroese L, et al. Reducing anastomotic leakage by reinforcement of colorectal anastomosis with cyanoacrylate glue. Eur Surg Res 2013;50:255-261.
[13] Vakalopoulos KA, Daams F, Wu Z, et al. Tissue adhesives in gastrointestinal anastomosis: a systematic review. J Surg Res 2013;180:290-300.
[14] Giuratrabocchetta S, Rinaldi M, Cuccia F, et al. Protection of intestinal anastomosis with biological glues: an experimental randomized controlled trial. Tech Coloproctol 2011;15:153-158.
[15] Stylianopoulos T, Aksan A, Barocas VH. A structural, kinetic model of soft tissue thermomechanics. Biophys J 2008;94:717-725.
[16] Wright N, Humphrey J. Denaturation of collagen via heating: an irreversible rate process. Annu Rev Biomed Eng 2002;4:109-128.
[17] Kramer EA, Rentschler ME. Energy-based tissue fusion for sutureless closure: applications, mechanisms, and potential for functional recovery. Annu Rev Biomed Eng 2018;20:1-20.
[18] Smulders J, De Hingh I, Stavast J, et al. Exploring new technologies to facilitate laparoscopic surgery: creating intestinal anastomoses without sutures or staples, using a radio-frequency-energy-driven bipolar fusion device. Surg Endosc 2007;21:2105-2109.
[19] Lim CBB, Goldin RD, Elson DS, et al. In vivo thermography during small bowel fusion using radiofrequency energy. Surg Endosc 2010;24:2465-2474.
[20] Salameh JR, Schwartz JH, Hildebrandt DA. Can LigaSure seal and divide the small bowel? Am J Surg 2006;191:791-793.
[21] Zhou H, Han S, Chen J, et al. A feasibility study of closing the small bowel with high-frequency welding device. J Biomed Eng 2014;31:1332-1335.
[22] Winter H, Holmer C, Buhr HJ, et al. Pilot study of bipolar radiofrequency-induced anastomotic thermofusion–exploration of therapy parameters ex vivo. Int J Colorectal Dis 2010;25:129-133.
[23] Zhao L, Zhuo C, Song C, et al. Histological characteristics of collagen denaturation and injuries in bipolar radiofrequency-induced colonic anastomoses. Pathol Res Pract 2015;211:214-218.
[24] Zhao L, Song C, Wang Z, et al. Novel concave–convex electrode for colonic anastomoses by radiofrequency thermo-fusion. Surg Endosc 2015;29:1809-1816.
[25] Tu L, Zhou Y, Song C, et al. Preliminary study of a control algorithm for radio-frequency-induced intestinal tissue fusion. Int J Hyperthermia 2019;36:1296-1305.
[26] Xing XP, Song CL. A novel electrode to achieve balance between anastomotic strength and tissue thermal damage for radiofrequency-induced intestinal anastomosis (Advance online publication). Acta Bioeng Biomech 2023;25(3).
[27] Dodde R, Bull J, Shih A. Bioimpedance of soft tissue under compression. Physiol Meas 2012;33:1095.
[28] Dodde RE, Miller SF, Geiger JD, et al. Thermal-electric finite element analysis and experimental validation of bipolar electrosurgical cautery. J Manuf Sci Eng 2008;130:021015.
[29] Trujillo M, Berjano E. Review of the mathematical functions used to model the temperature dependence of electrical and thermal conductivities of biological tissue in radiofrequency ablation. Int J Hyperthermia 2013;29:590-597.
[30] Zhang C, Liu H, Tan R, et al. Interaction model between capsule robot and intestine based on nonlinear viscoelasticity. Proc Inst Mech Eng H 2014;228:287-296.
[31] Pennes HH. Analysis of tissue and arterial blood temperatures in the resting human forearm. J Appl Physiol 1948;1:93-122.
[32] Pearce JA. Comparative analysis of mathematical models of cell death and thermal damage processes. Int J Hyperthermia 2013;29:262-280.
[33] Rosendorf J, Klicova M, Herrmann I, et al. Intestinal anastomotic healing: what do we know about processes behind anastomotic complications. Front Surg 2022;9:904810.
[34] Richter S, Kollmar O, Schilling M, et al. Efficacy and quality of vessel sealing: comparison of a reusable with a disposable device and effects of clamp surface geometry and structure. Surg Endosc 2006;20:890-894.